# Design and development of a coaxial cryogenic probe for precision measurements of the quantum Hall effect in the AC regime

*Original*
Design and development of a coaxial cryogenic probe for precision measurements of the quantum Hall effect in the AC regime / Marzano, Martina; Tran, Ngoc Thanh Mai; D'Elia, Vincenzo; Serazio, Danilo; Enrico, Emanuele; Ortolano, Massimo; Pierz, Klaus; Kucera, Jan; Callegaro, Luca. - In: ACTA IMEKO. - ISSN 2221-870X. - 10:2(2021), p. 24. [10.21014/acta_imeko.v10i2.925]

*Availability:*
This version is available at: 11696/73322 since: 2022-02-21T09:54:35Z

*Publisher:*
Imeko

*Published*
DOI:10.21014/acta_imeko.v10i2.925

Figure 1. A computer rendering of the cryomagnetic probe assembly: (left) side view; (right) front view, showing the magnet bore.

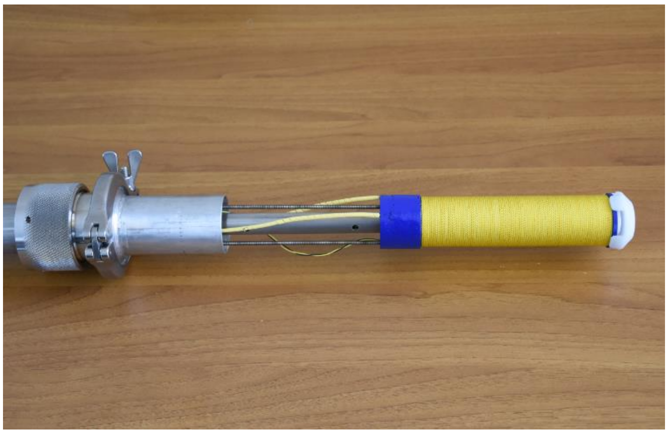

Figure 2. The probe cryomagnet, showing the yellow winding insulation. A header (white) was added to ease the insertion in the cryostat.

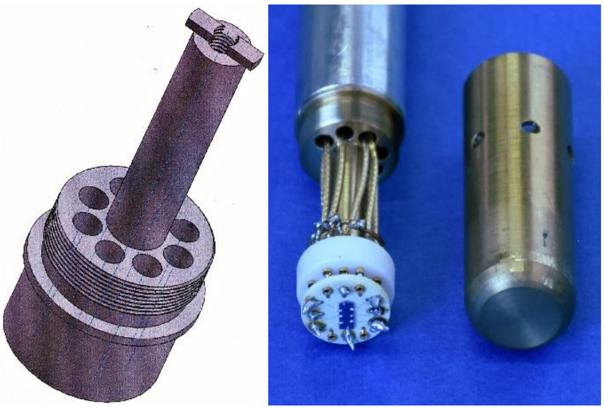

Figure 3. The bottom side of the insert, which slides into the cryomagnet bore. (left) Diagram of the drum that supports the sample holder and hosts the 9 coaxial connections. (right) Photo of the assembled probe: the brass shield (right) has been removed to show the TO-8 socket, which hosts a GaAs device on its TO-8 holder, and the 9 coaxial electrical lines.

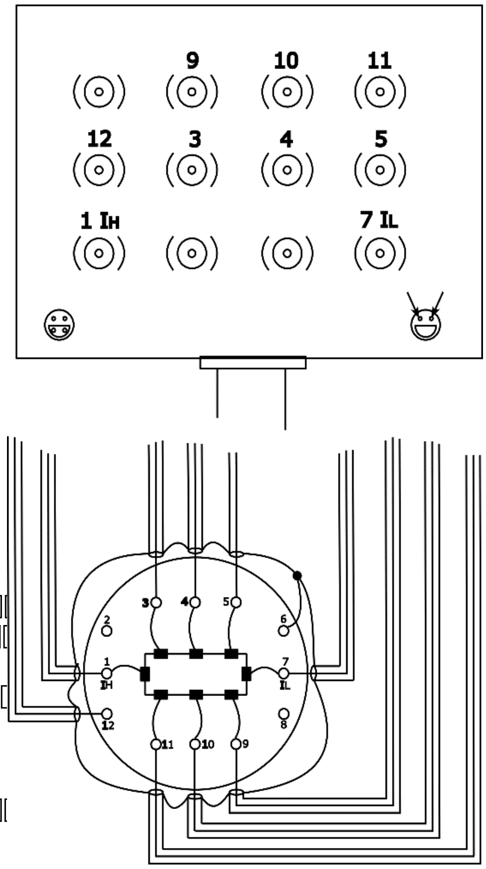


Figure 5. Schematic diagram of the coaxial connections of the probe. Nine coaxial connections are available, fully isolated from the probe metal bulk. The outer conductors of each line are joined together on the sample holder (pin 6).

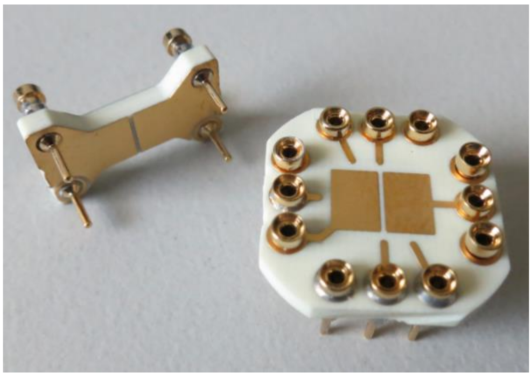

Figure 4. TO-8 sample holders, implementing the double-shielding technique [8], [17]. After the bonding of the quantum Hall device onto the holder (right), the shielding cap (left) slids into the socket.

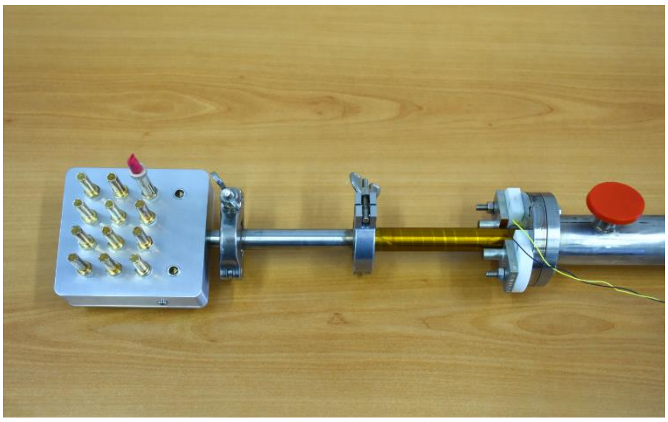

Figure 6. The probe connection box.

[illegible]

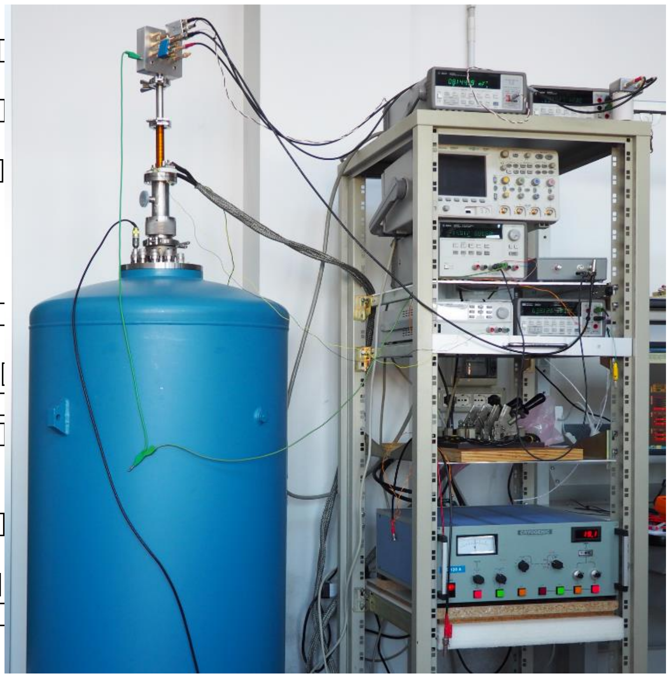

Figure 7. Overall view of the measurement setup for DC characterization. On the left, the liquid helium dewar, with the coaxial probe inserted. On the right, the rack of electronic instrumentation.

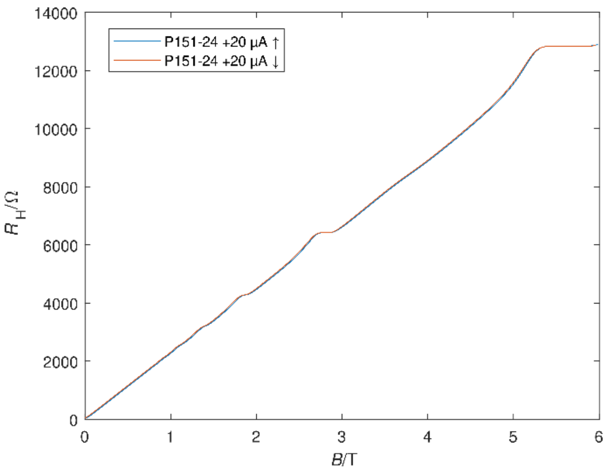


(a) $R_H(B)$

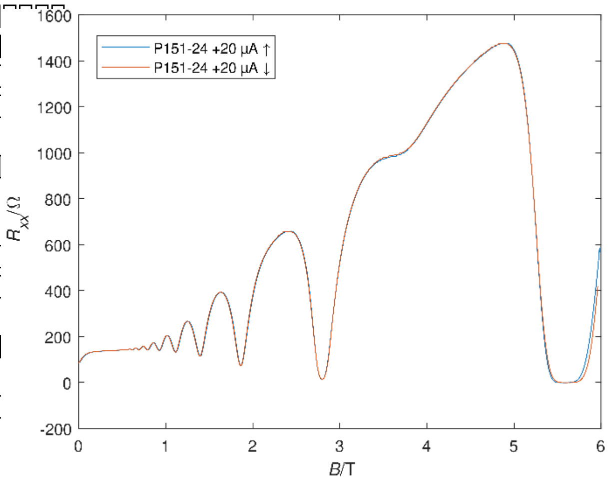


(b) $R_{xx}(B)$

Figure 8. Plot of the measured values of $R_H$ and $R_{xx}$ versus the magnetic field $B$, for an applied current $I$ = 20 µA. Blue line: increasing magnetic field. Red line: decreasing magnetic field.

Table 1. Calculation of the real part of the relative error $\delta Z_{\mathrm{H}}$ occurring when measuring a QHE device by using the $n$-series connections given in Figure 9, for the frequency $f$ = 1541 Hz. The calculation is given for two different contact resistance values.

| $\delta Z$ | $n$ | $R$ = 10 mΩ | $R$ = 10 Ω |
|---|---|---|---|
| | 1 | $+1.0 \times 10^{-4}$ | $+1.7 \times 10^{-3}$ |
| | 2 | $-5.6 \times 10^{-9}$ | $+1.4 \times 10^{-6}$ |
| | 3 | $-1.1 \times 10^{-8}$ | $-9.5 \times 10^{-9}$ |

$$\delta Z_{\mathrm{H}} = \frac{Z_{\mathrm{H}} - R_{\mathrm{H}}}{R_{\mathrm{H}}},$$

$$\delta Z_{\mathrm{H}} \approx \left[\frac{Z_{\mathrm{w}} Y_{\mathrm{w}}}{2} + \left(\frac{R_{\mathrm{c}} + R_{\mathrm{w}}}{R_{\mathrm{H}}}\right)^{n}\right]^{2}.$$

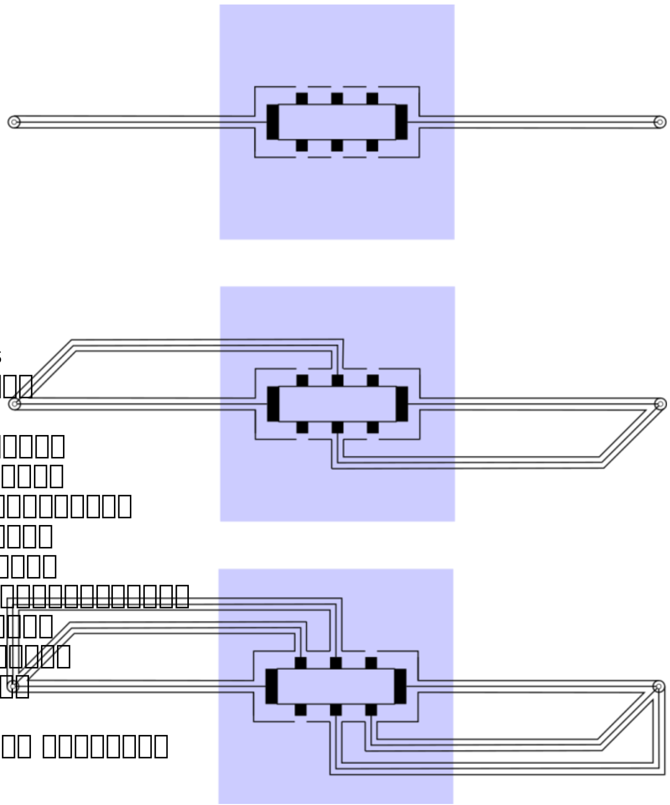

Figure 9. $n$-series connection of a QHE device. (top) $n$ = 1, no multiple-series connection: the device is connected as a 2TP impedance by two coaxial leads. (middle) $n$ = 2, double-series connection. (low) $n$ = 3, triple-series connection.

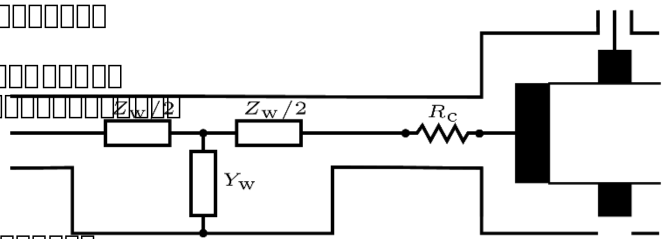


Figure 10 Electrical modelling of one of the connections to the QHE device. In the AC regime, each connection is modelled as a T network with series impedance $Z_{\mathrm{w}}$ and a parallel admittance $Y_{\mathrm{w}}$. The contact resistance $R_{\mathrm{C}}$ models the bonding and the device junctions.

GIQS: Graphene Impedance Quantum Standard


&DOOHJDUR 9 '•(OLD 0 .DPSLN ' 9

0 0DU]DQR 0 2UWRODQR 9 '•(OLD $